Effective diffusion tensor computed by homogenization

Dang Van Nguyen, Jing-Rebecca Li, Denis Grebenkov, Cyril Poupon, Denis Le Bihan

Effective diffusion tensor computed by homogenization

Dang Van Nguyen[1], Denis Grebenkov[2], Cyril Poupon[3], Denis Le Bihan[3], and Jing-Rebecca Li[4]

[1]CMAP, Ecole Polytechnique, Palaiseau, France, [2]LPMC, CNRS – Ecole Polytechnique, Palaiseau, France, [3]Neurospin, CEA Saclay, Gif-sur-Yvette, France, [4]Equipe DEFI, INRIA Saclay, Palaiseau, France

Corresponding author: Dang Van Nguyen, E-Mail: vdnguyen@cmap.polytechnique.fr

Abstract

The convergence of the long-time apparent diffusion tensor under realistic DMR scanning conditions to the effective diffusion tensor obtained by homogenization theory was considered for a two-compartment model in both isotropic and anisotropic diffusion and general shapes. This gives a computationally efficient approach to get the homogenized diffusion tensor.

Keywords

Effective diffusion tensor, apparent diffusion tensor, two-compartment model, Bloch-Torrey equation, Laplace equation.

1. Introduction

Diffusion magnetic resonance imaging (DMRI) can give useful information on cellular structure and structural changes [1]. We show that the effective diffusion tensor obtained by mathematical homogenization theory [2,3] is a good approximation to the long time apparent diffusion tensor under realistic DMR scanning conditions of a two-compartment model for both isotropic and anisotropic diffusion and general shapes. The homogenized diffusion tensor is obtained by solving d steady-state Laplace equations (where $d = 2,3$ is the problem dimension), which is a more computationally efficient approach than long time simulation in the time domain, either via Monte-Carlo simulation or numerical solution of the time-dependent Bloch-Torrey PDE.

2. Theory

We consider two compartments, Ω^{in} and Ω^{ex}, to be an ensemble of cells and the extra-cellular space, respectively, with the same intrinsic diffusion coefficient D. The cell membrane is modeled by an infinitely thin permeable interface Γ characterized by permeability κ. Fig. 1 illustrates a 2D sample in which the union of blue cells is considered as the interior compartment and the remaining part is the exterior one.

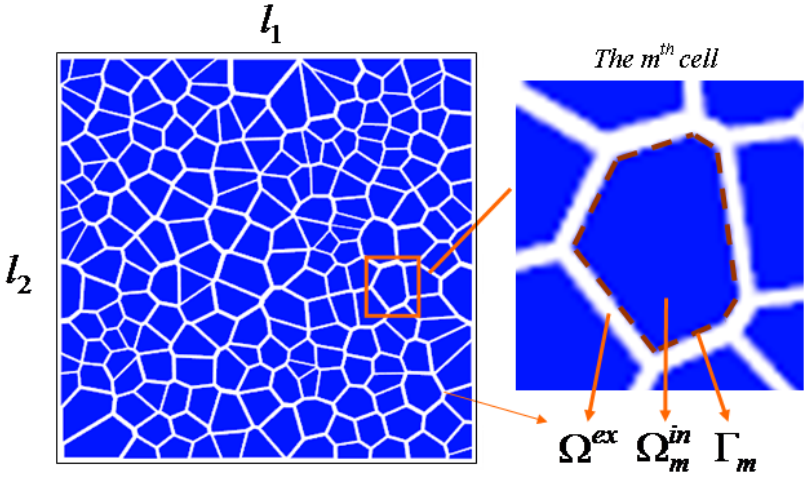

Fig. 1: A two-compartment model with the extracellular Ω^{ex} *(white region), the intracellular compartment* $\Omega^{in} = \cup_m \Omega_m^{in}$ *(blue regions) and the interface* $\Gamma = \cup_m \Gamma_m$

For a given diffusion gradient with the temporal profile $f(t)$ and gradient strength $\vec{g} := \vec{q} / \gamma$ (here γ is the gyromagnetic ratio), the transverse magnetization is described by the two-compartment Bloch-Torrey partial differential equation (PDE) [4]

$$\frac{\partial M(\vec{x},t)}{\partial t} = -i\gamma f(t)(\vec{g}\cdot\vec{x}) M(\vec{x},t) + \nabla\left(D\nabla M(\vec{x},t)\right)$$

with the interface conditions at the inter-compartment interface Γ,

$$D\nabla M^{in}(\vec{x},t)\cdot\vec{n}^{in}(\vec{x}) = -D\nabla M^{ex}(\vec{x},t)\cdot\vec{n}^{ex}(\vec{x}) = \kappa(M^{ex}(\vec{x},t) - M^{in}(\vec{x},t)), \quad \vec{x}\in\Gamma,$$

(here $\vec{n}^{ex}$ and $\vec{n}^{in}$ are normal vectors at Γ pointing outward Ω^{ex} and Ω^{in}, respectively), and the boundary conditions at the exterior boundaries of the computational box $\Omega = \prod_{k=1}^{d}[a_k, b_k]$, $(a_k < b_k)$ which contains a representative sample of the cellular structure:

$$\left[M(\vec{x},t)\right]_{x_k=a_k} = \left[M(\vec{x},t)\right]_{x_k=b_k} \exp\left(i(\vec{g}\cdot\vec{e}_k)\gamma l_k \int_0^t f(s)\,ds\right)$$

$$\left[\frac{\partial M(\vec{x},t)}{\partial x_k}\right]_{x_k=a_k} = \left[\frac{\partial M(\vec{x},t)}{\partial x_k}\right]_{x_k=b_k} \exp\left(i\gamma(\vec{g}\cdot\vec{e}_k) l_k \int_0^t f(s)\,ds\right)$$

where $l_k = b_k - a_k, k = 1..d$ and $\vec{x} = (x_1,..,x_d)$ is the spatial position.

For the uniform initial condition, the DMRI signal is $\Psi(\vec{q},t) = \int_\Omega M(\vec{x},t)\,d\vec{x}$. From the Taylor expansion of the DMRI signal in $\vec{q}$, we define the apparent diffusion tensor D^A which may depend on time t:

$$\ln\Psi(\vec{q},t) = -\vec{q}^T D^A \vec{q} \int_0^t du\left(\int_0^u f(s)ds\right)^2 + O\left(\|\vec{q}\|^4\right)$$

The long time limit of D^A can be approximated by the effective diffusion tensor obtained from homogenization theory [6], $D^{eff} = \left[D_{jk}^{eff}\right]_{j=1..d,k=1..d}$, where $D_{jk}^{eff} = D\int_\Omega \nabla v_j\cdot\vec{e}_k\,d\vec{x}$, $\vec{e}_k$ is the unit vector in the k^{th} coordinate direction and the unknown functions v_j can be found by solving the Laplace equation

$$-\nabla\left(D\nabla v_j(\vec{x})\right) = 0$$

with the interface conditions at the inter-compartment interface Γ ,

$$D\nabla v_j^{in}(\vec{x})\cdot\vec{n}^{in}(\vec{x}) = -D\nabla v_j^{ex}(\vec{x})\cdot\vec{n}^{ex}(\vec{x}) = \kappa(v_j^{ex}(\vec{x}) - v_j^{in}(\vec{x})),\quad \vec{x}\in\Gamma\ ,$$

and the boundary conditions at the exterior boundaries of the computational box Ω are

$$\left[v_j(\vec{x})\right]_{x_k=a_k} = \left[v_j(\vec{x})\right]_{x_k=b_k} - (\vec{g}\cdot\vec{e}_k)\,l_k\ ,$$

$$\left[\frac{\partial v_j(\vec{x})}{\partial x_k}\right]_{x_k=a_k} = \left[\frac{\partial v_j(\vec{x})}{\partial x_k}\right]_{x_k=b_k}$$

3. Results

We performed simulations on the computational domain $[-10\,\mu m, 10\,\mu m]^d$ containing numerous convex cells . To construct these samples, we randomly generated a set of segments in 2D (Fig. 3) and a set of faces in 3D (Fig. 5). Since the boundaries should be periodic, we mirrored this set across all coordinate axes. Then, each segment (face) was thickened to create an extracellular compartment Ω^{ex} . The interior compartment Ω^{in} includes polygonal cells. The same intrinsic diffusion coefficient of water molecules $D = 3\cdot 10^{-3}\ \frac{\mu m^2}{\mu s}$ was set for both interior and exterior compartments. Two values of permeability, $\kappa = 10^{-5}\ \frac{\mu m}{\mu s}$ and $\kappa = 10^{-4}\ \frac{\mu m}{\mu s}$, were considered.

The Bloch-Torrey equation was solved for Stejskal - Tanner PGSE sequences (Fig. 2) with two rectangular gradient pulses of duration $\delta = 10\,ms$ and severals diffusion times Δ to obtain the signal attenuation $\Psi(\vec{q},t)$ at some b-values:

$$b = \vec{q}^{\,T}\vec{q}\int_0^t du\left(\int_0^u f(s)ds\right)^2 = \gamma^2\left\|\vec{g}\right\|^2\delta^2\left(\Delta - \frac{\delta}{3}\right).$$

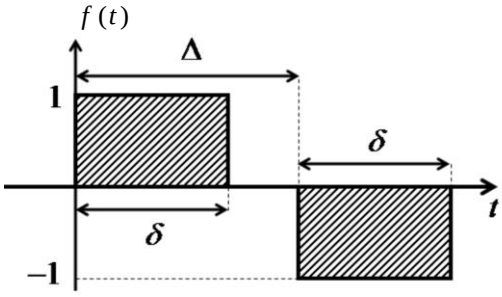

Fig.2: Stejskal-Tanner PGSE

Then, the entries of D^A appear in front of the first-degree term of the polynomial fit of $-\ln\Psi(\vec{q},t)$ versus b-value. The Laplace equation was also solved over the same box to obtain D^{eff} .

All computations were carried out on a Dell Latitiude E6410 laptop computer.

2D results

The 2D sample was created by 20 thick segments that divide the computational domain into 116 convex cells (Fig. 3). The volume fraction v^i is *0,77* , the average radius of cells is *1,2* μm and the average surface to volume ratio *S/V* is *0,41* μm^{-1}.

We performed the simulations for two gradient directions [1,0] and [0,1]. Each D^A was computed from 7 b-values changing from 0 to $4000\ \frac{\mu s}{\mu m^2}$ for $\kappa = 10^{-5}\ \frac{\mu m}{\mu s}$ and from 0 to $3000\ \frac{\mu s}{\mu m^2}$ for $\kappa = 10^{-4}\ \frac{\mu m}{\mu s}$ that took between 15 and 30 minutes for the mesh size of 33813 vertices. On the contrary, it took only a few seconds to compute each D^{eff} .

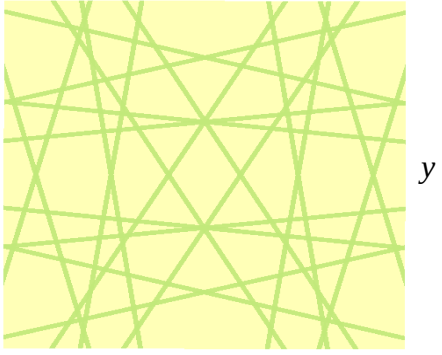

Fig.3: 2D sample

Fig. 4 shows the convergence of D^A to D^{eff} for the first direction [1,0] and the permeability $\kappa = 10^{-5}\ \frac{\mu m}{\mu s}$ with 10 values of diffusion time Δ changing from 10ms to 190ms. We plot here the diffusion coefficient versus Δ^{-1}.

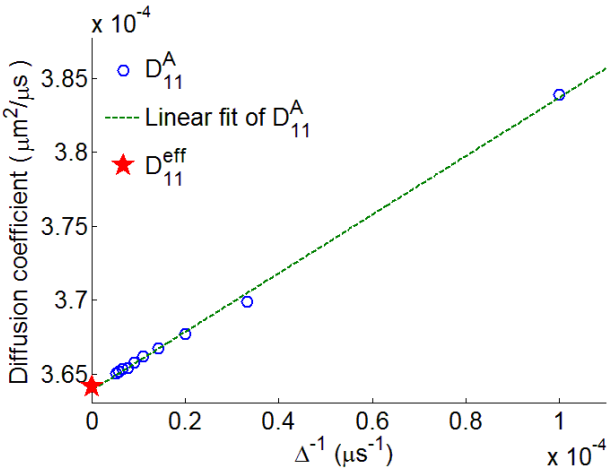

Fig.4: The convergence of D^A to D^{eff} in 2D for the direction [1,0] and $\kappa = 10^{-5}\ \frac{\mu m}{\mu s}$.

The blue circles represents D^A, the dashed line shows a linear fit of D^A versus Δ^{-1}, and the red star indicates D^{eff}.

Results for two gradient directions with Δ =10ms, 50ms and 190ms are summarized in the following table:

	$\kappa=10^{-4}$ µm/µs				$\kappa=10^{-5}$ µm/µs			
	$\vec{q}^{\,t} D^A \vec{q}$			$\vec{q}^{\,t} D^{eff} \vec{q}$	$\vec{q}^{\,t} D^A \vec{q}$			$\vec{q}^{\,t} D^{eff} \vec{q}$
$\vec{q}/\|\vec{q}\|$	Δ=10	Δ=110	Δ=190		Δ=10	Δ=110	Δ=190	
(1,0)	$5{,}33\cdot10^{-4}$	$5{,}24\cdot10^{-4}$	$5{,}23\cdot10^{-4}$	$5{,}22\cdot10^{-4}$	$3{,}84\cdot10^{-4}$	$3{,}66\cdot10^{-4}$	$3{,}65\cdot10^{-4}$	$3{,}64\cdot10^{-4}$
(0,1)	$5{,}69\cdot10^{-4}$	$5{,}61\cdot10^{-4}$	$5{,}60\cdot10^{-4}$	$5{,}59\cdot10^{-4}$	$4{,}06\cdot10^{-4}$	$3{,}95\cdot10^{-4}$	$3{,}94\cdot10^{-4}$	$3{,}93\cdot10^{-4}$

3D results

The 3D sample was created by 16 thick faces which cut the cube into 80 cells (Fig. 5). The average radius of cells is $2{,}5\ \mu m$, volume fraction $v^i = 0{,}66$ and the average surface to volume ratio S/V is $0{,}29\ \mu m^{-1}$.

The simulations were performed for three gradient directions [1,0,0], [0,1,0] and [0,0,1]. Each D^A was computed at 9 b-values changing from 0 to 3000 $\frac{\mu s}{\mu m^2}$ for $\kappa = 10^{-5}\ \frac{\mu m}{\mu s}$ and from 0 to 2000 $\frac{\mu s}{\mu m^2}$ for $\kappa = 10^{-4}\ \frac{\mu m}{\mu s}$. The computation took between 30 minutes and 2 hours to compute each D^A. On the contrary, it took less than one minute to compute D^{eff} for the mesh size of 50476 vertices.

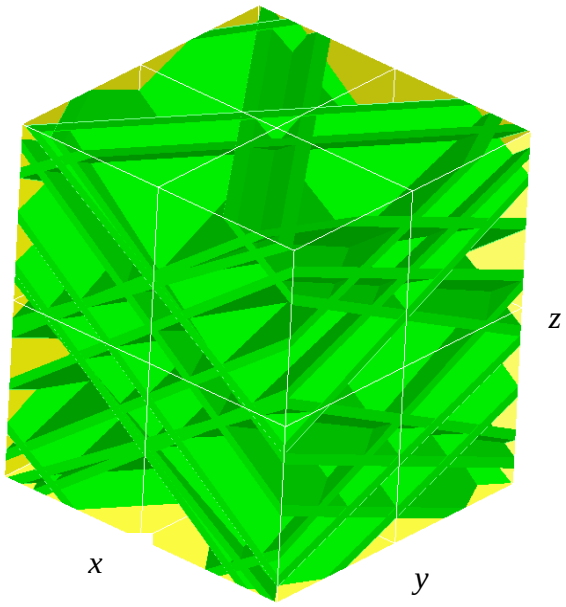

Fig.5: 3D sample

Five values of the diffusion time Δ, 10ms, 30ms, 50ms and 90ms, were chosen to study the convergence of D^A to D^{eff} for the first direction [1,0,0] and $\kappa = 10^{-5}\frac{\mu m}{\mu s}$. The corresponding D^A was showed in term of Δ^{-1} in Fig. 6.

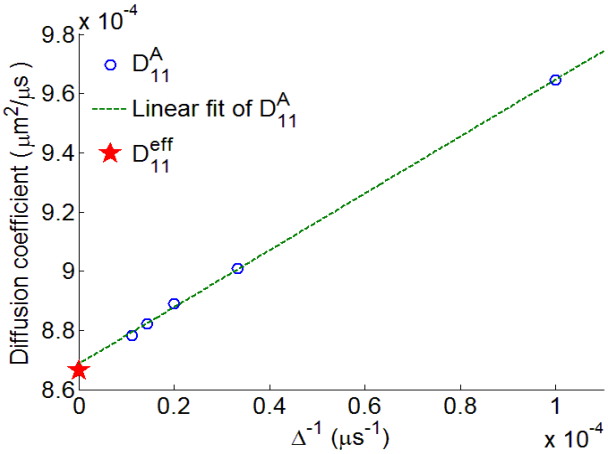

Fig. 6: The convergence of D^A to D^{eff} in 3D for the direction [1,0,0] and $\kappa = 10^{-5}\frac{\mu m}{\mu s}$. The blue circles represents D^A, the dashed line shows a linear fit of D^A versus Δ^{-1}, and the red star indicates D^{eff}.

Results for three gradient directions with Δ =10ms, 50ms and 90ms are summarized in the following table:

	$\kappa=10^{-4}$ μm/μs				$\kappa=10^{-5}$ μm/μs			
	$\vec{q}^{\,t} D^A \vec{q}$			$\vec{q}^{\,t} D^{eff} \vec{q}$	$\vec{q}^{\,t} D^A \vec{q}$			$\vec{q}^{\,t} D^{eff} \vec{q}$
$\vec{q}/\|\vec{q}\|$	Δ=10	Δ=50	Δ=90		Δ=10	Δ=50	Δ=90	
(1,0,0)	$1{,}24\cdot10^{-3}$	$1{,}22\cdot10^{-3}$	$1{,}22\cdot10^{-3}$	$1{,}21\cdot10^{-3}$	$9{,}65\cdot10^{-4}$	$8.89\cdot10^{-4}$	$8.78\cdot10^{-4}$	$8{,}66\cdot10^{-4}$
(0,1,0)	$1{,}73\cdot10^{-3}$	$1{,}67\cdot10^{-3}$	$1{,}67\cdot10^{-3}$	$1{,}66\cdot10^{-3}$	$1{,}26\cdot10^{-3}$	$1{,}11\cdot10^{-3}$	$1{,}09\cdot10^{-3}$	$1{,}07\cdot10^{-3}$
(0,0,1)	$6{,}89\cdot10^{-4}$	$6{,}87\cdot10^{-4}$	$6{,}85\cdot10^{-4}$	$6.85\cdot10^{-4}$	$5{,}01\cdot10^{-4}$	$4{,}93\cdot10^{-4}$	$4{,}92\cdot10^{-4}$	$4{,}91\cdot10^{-4}$

4. Conclusions

The long-time apparent diffusion tensor D^A approaches the steady-state tensor D^{eff} computed by the homogenization in both cases of isotropic and anisotropic diffusion and the convergence is faster at higher permeability. This convergence seems to be linear in term of Δ^{-1} that agrees with the result for 1D periodic structure in the long-time regime [7]. The computation of D^{eff} is very much faster than that of D^A. Since the samples were generated randomly, this conclusion is expected to be valid for general shapes.

References

[1] LeBihan (2007) Phys Med Bio 52.
[2] Bensoussan et al. (1978) Asymptotic analysis for periodic structures, North-Holland, Amsterdam.
[3] Cheng et al. (1997) Proc Math Phy Engin Sci 453:145–161.
[4] Grebenkov (2007) Rev Mod Phys 79, 1077–1137.
[5] Novikov et al. (2011) Nature Physics 7, 508–514.
[6] J.R Li et al. (in preparation) Numerical and analytical models of the long time apparent diffusion tensor.
[7] Dmitriy A.Yablonskiy et al. (2010) NMR Biomed 23, 661–681.